Journal of Alloys and Compounds 486 (2009) 9–13

Contents lists available at ScienceDirect

Journal of Alloys and Compounds

journal homepage: www.elsevier.com/locate/jallcom

Structure and optical properties of nanocrystalline NiO thin film synthesized by sol–gel spin-coating method

A.A. Al-Ghamdi[a], Waleed E. Mahmoud[a,b,*], S.J. Yaghmour[a], F.M. Al-Marzouki[a]

[a] King Abdulaziz University, Faculty of Science, Physics Department, Jeddah, Saudi Arabia
[b] Suez Canal University, Faculty of Science, Physics Department, Ismailia, Egypt

ARTICLE INFO

Article history:
Received 21 May 2009
Received in revised form 21 June 2009
Accepted 22 June 2009
Available online 30 June 2009

Keywords:
NiO
Sol–gel
Spin coating
Structure
Optical properties

ABSTRACT

NiO thin film was prepared by sol–gel spin-coating method. This thin film annealed at $T = 600\,^{\circ}\mathrm{C}$. The structure of NiO thin film was investigated by means of X-ray diffraction (XRD) technique and scanning electron microscopy (SEM). The optical properties of the deposited film were characterized from the analysis of the experimentally recorded transmittance and reflectance data in the spectral wavelength range of 300–800 nm. The values of some important parameters of the studied films are determined, such as refractive index (n), extinction coefficient (k), optical absorption coefficient (α) and band energy gap (E_g). According to the analysis of dispersion curves, it has been found that the dispersion data obeyed the single oscillator of the Wemple–DiDomenico model, from which the dispersion parameters and high-frequency dielectric constant were determined. In such work, from the transmission spectra, the dielectric constant (ε_∞), the third-order optical nonlinear susceptibility $\chi^{(3)}$, volume energy loss function (VELF) and surface energy loss function (SELF) were determined.

1. Introduction

Recently, nanomaterials have attracted extensive interest because of their unique properties in various fields in comparison with their bulk counterparts [1]. A reduction in particle size to nanometer scale results in various interesting properties compared with their bulk properties. Having a large surface area, metal oxide nanomaterials show great advantages over conventional materials in many applications. Transparent semiconducting materials, which can be grown efficiently as thin films with low cost, are used extensively for a variety of applications, including architectural windows, solar cells, heat reflectors, light transparent electrodes, and thin-film photovoltaic and many other opto-electronic devices.

Nanosized nickel oxide has demonstrated excellent properties such as catalytic [2], magnetic [3], electrochromic [4], optical and electrochemical properties [5]. Furthermore, nickel oxides can be used as a transparent p-type semiconducting layer [6] and are being studied for applications in smart windows, electrochemical supercapacitors [7] and dye sensitized photocathodes [8]. A variety of strategies have been employed for synthesis and manipulation of nanostructured nickel oxide, such as evaporation [9], sputtering [10], electrodeposition [11], thermal decomposition [12] and sol–gel techniques [13]. Thermal decomposition method has some advantages such as simple process, low cost and easiness to obtain high purity products hence it is quite promising and facile rout for industrial applications.

In the present work, the structure properties of NiO thin film prepared by sol–gel spin coating have been studied. The absorption spectra are also measured in the wavelength range 300–800 nm. In addition, the optical constants (n and k) are determined from the transmittance T and the reflectance R of the film in the spectral range from 300 to 800 nm. The transport and the onset energy gap are also estimated.

2. Experimental

NiO film was deposited onto glass substrates by the sol–gel method using a spin-coating technique [13]. Nickel acetate [$Ni(CH_3COO)_2\cdot 4H_2O$] was used as a starting material. 2-Methoxethanol ($C_3H_8O_2$) and monoethanolamine (C_2H_7NO, MEA) were used as a solvent and stabilizer, respectively. 2 mmol of nickel acetate was dissolved into 20 ml of 2-methoxethanol then MEA added to them. The molar ratio of MEA to nickel acetate was maintained at 1:1. The obtained mixture was stirred at $60\,^{\circ}\mathrm{C}$ for 2 h to yield a clear and homogeneous solution and then it was served as the coating source after cooling down to room temperature. The glass substrates were first cleaned by detergent, and then in methanol and acetone each for 10 min by using ultrasonic cleaner. At last, the substrates were rinsed with deionized water and dried with nitrogen. The coating solution was dropped into glass substrate, which was rotated at 3000 rpm for 30 s using spin coater. After the spin coating, the film was dried at $200\,^{\circ}\mathrm{C}$ for 15 min in a furnace to evaporate the solvent and to remove organic residuals, and then annealed at $600\,^{\circ}\mathrm{C}$ in air for 30 min.

The structural characteristics of NiO film were investigated by X-ray diffraction patterns. Philips X-ray diffractometer (model X' Pert) was used for the measurement of utilized monochromatic CuKα radiation operated at 40 kV and 25 mA. The diffrac-

* Corresponding author at: Suez Canal University, Faculty of Science, Physics Department, Ismailia, Egypt. Tel.: +20 16 2277227.
E-mail address: w_e_mahmoud@yahoo.com (W.E. Mahmoud).

0925-8388/$ – see front matter © 2009 Elsevier B.V. All rights reserved.
doi:10.1016/j.jallcom.2009.06.139

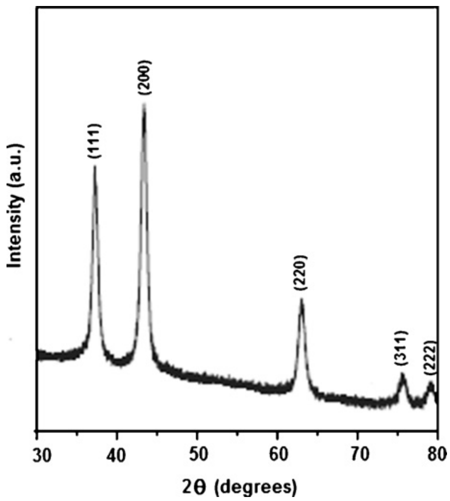

Fig. 1. XRD of NiO thin film annealed at 600 °C.

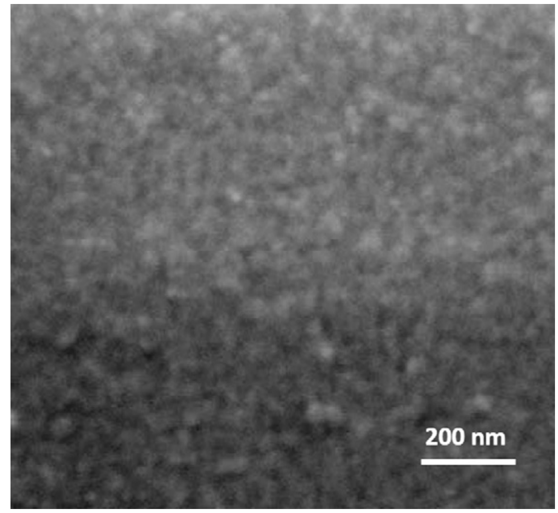

Fig. 2. SEM photography of NiO thin film annealed at 600 °C.

tion patterns were recorded automatically with a scanning speed of 2° min^{-1}. UV–vis absorption spectra of NiO film, deposited onto optically flat fused quartz substrates, were recorded on spectrophotometer. In addition, *T* and *R* of the annealed film were measured at normal incidence in the spectral ranging from 300 to 800 nm. This is by using a double-beam spectrophotometer (JASCO model V-570 UV–vis–NIR) attached with constant angle specular reflection attachment (5°).

3. Results and discussions

3.1. Structural properties

Fig. 1 shows the X-ray diffraction (XRD) pattern of NiO thin film annealed at 600 °C for 30 min. The observed indexed peaks in this XRD pattern are fully matched with the corresponding pure cubic-structured crystalline NiO. Several peaks are observed in the pattern at 2θ = 37.1°, 43.3°, 62.8°, 75.2°, and 79.3° assigned to the (1 1 1), (2 0 0), (2 2 0), (3 1 1) and (2 2 2) crystal planes, respectively. The indexed peaks are fully consistent with the cubic-structured crystalline NiO (JCPDS 47-1049) [14]. In addition to this, no peaks for any impurities such as α-$Ni(OH)_2$, β-$Ni(OH)_2$, or other phases were observed in the pattern which further confirm the crystalline and pure phase of the cubic NiO. Moreover, the observed peaks are sharper and higher in intensity which confirmed the well-crystallization of the obtained NiO structures. The average diameter was calculated by using Scherrer formula [15]

$$d = \frac{k\lambda}{\beta\cos\theta} \tag{1}$$

where k is a constant which is taken to be 0.9, λ the wavelength of X-rays used (0.1789 nm), β the full width at half maximum (FWHM) and θ is the angle of diffraction. The average diameter of NiO nanoparticles was found to be about 25 nm.

The surface morphology of the as-prepared NiO nanoparticle film, annealed at 600 °C for 30 min, has been studied by scanning electron microscopy (SEM), Fig. 2. It is clearly observed from the micrography that the nanoparticles are extra-fine, and uniformly distributed on the glass substrate.

3.2. Optical properties

The analysis of optical absorption spectra is one of the most productive tools for understanding and developing the band structure and energy band gap, E_g, of crystalline structure. Fig. 3 shows the dependence of absorption on the wavelength λ in the spectral range 300–800 nm for NiO thin film. From such figure it is clear that, there is absorption peak at 320 nm due to interband π–π^* electronic transition. The band-gap value could be obtained from the optical absorption spectra by using Tauc's relation [16];

$$\alpha = \frac{A}{h\upsilon}(h\upsilon - E_g)^n \tag{2}$$

where α is the absorption coefficient $(h\nu)$ is the photon energy, A is a constant and n assumes the values 1/2, 2, 3/2 and 3 for allowed direct, allowed indirect, forbidden direct and forbidden indirect transitions, respectively. Now for allowed direct type of transitions.

$$\alpha h\upsilon = A(h\upsilon - E_g)^{1/2} \tag{3}$$

Fig. 4 shows the variation of $(\alpha h\nu)^2$ versus $(h\nu)$ for the NiO thin film. The straight line nature of the plots over a wide range of photon energy indicates the direct type of transition. The optical gap has then been determined by the extrapolation of the linear region on the energy axis as shown in Fig. 4. The optical gap for NiO film was found to be 3.44 eV.

The average radius of NiO nanoparticles can be estimated in the effective mass approximation [17]:

$$\Delta E_g = \frac{\hbar^2\pi^2}{2R^2}\left(\frac{1}{m_e^*} + \frac{1}{m_h^*}\right) \tag{4}$$

where ΔE_g is the difference between the NiO nanoparticles E_g value and the energy position of the long-wave edge of the absorption band of NiO film and m_e^* (=0.11 m_o) and m_h^* (=0.32 m_o) [18] the effective masses of the conduction band electrons and the valence band holes of NiO, respectively. Using the above equation, the particle

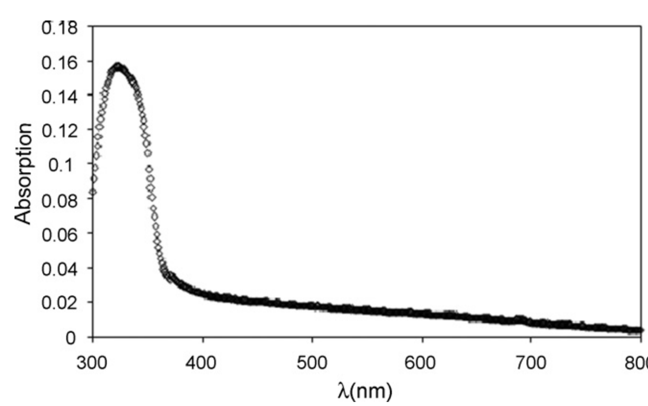

Fig. 3. Absorption spectrum of NiO thin film.

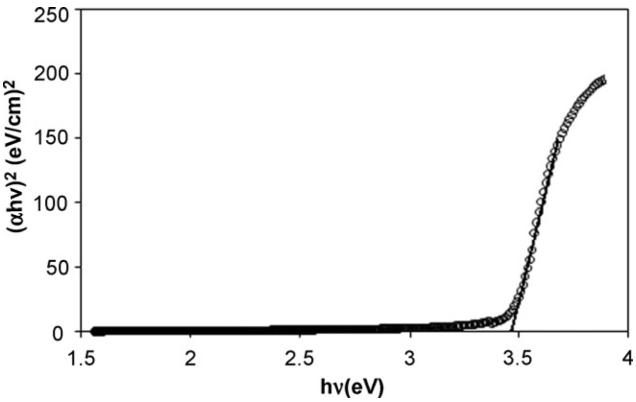

Fig. 4. The variation of $(\alpha h\nu)^2$ versus $(h\nu)$ for NiO thin film.

size of NiO nanoparticles has been estimated which found to be 24.5 nm. This value is in good agreement with that obtained from XRD data.

The transmittance and reflectance spectra of the NiO film were measured to investigate the optical properties of the films and are presented in Fig. 5. This figure depicts that the NiO film is highly transparent and has an average transmittance within region 95–98% in the visible region. As seen in Fig. 5, in the visible region, the reflectance is limited only by the surface reflectance of about 2–5%.

The refractive index of the films was calculated by the following relation [19],

$$n = \left(\frac{1+R}{1-R}\right) - \sqrt{\frac{4R}{(1-R)^2} - k^2} \tag{5}$$

where R is the reflectance and k ($k = \alpha\lambda/4\pi$) is the extinction coefficient. The absorption coefficient α [20] has been determined from the spectra using the formula ($\alpha = \ln(1/T)/d$), where T is the transmittance and d is the thickness of the film (=100 nm).

Fig. 6 shows the refractive index, n, and extinction coefficient, k, of NiO film as a function of wavelength. The dispersion curve of refractive index is fairly flat in the long wavelength region and rises rapidly towards shorter wavelengths, showing the typical shape of dispersion curve near an electronic interband transition. This suggests that the film shows normal dispersion. The refractive index is between 2.3 and 1.95 in the visible region. The extinction coefficient decreases gradually with the shortening of wavelength. The calculated k value included the total optical losses caused by both absorption and scattering waves, this factor average is 1.2×10^{-2} at visible range. The low value of extinction coefficient is in the order

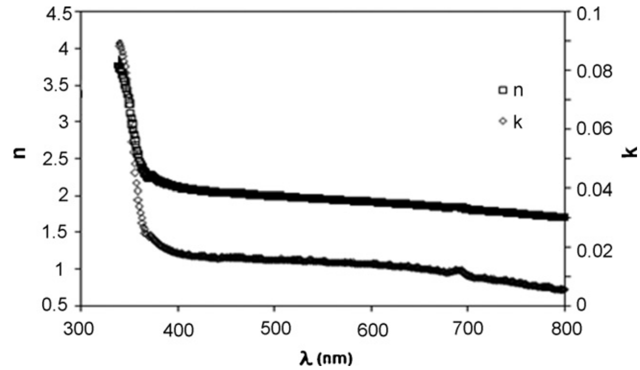

Fig. 6. The refractive index (n) and extinction coefficient (k) of NiO film as a function of wavelength.

of 10^{-2} in visible region, it is a qualitative indication of excellent surface smoothness of the NiO thin film [21].

In the normal dispersion region above ($\lambda > 320$ nm), the refractive index dispersion is analyzed by using Wemple and DiDomenico single oscillator model [22]. In terms of this model, the refractive index as a function of photon energy can be expressed in the form:

$$\frac{1}{n^2-1} = \left(\frac{E_o}{E_d}\right) - \left(\frac{1}{E_o E_d}\right)(h\nu)^2 \tag{6}$$

where h is the Planck constant, ν is the frequency, E_o is the oscillator energy and E_d is the dispersion energy, which is the measure of the average strength of interband optical transition or the oscillator strength. The single oscillator energy E_o and the dispersion energy E_d can be obtained from Eq. (6) by plotting $(n^2-1)^{-1}$ against $(h\nu)^2$ as shown in Fig. 7. The determination of E_o and E_d can be made from the plot, using the linear fit parameters. The values of E_d and E_o are obtained from the intercepts and the slopes of the curves. The oscillator energy, E_o, is related to the optical band gap, E_g is in close approximation by $E_o = 2E_g$. Using the curve above the estimated values of the oscillator parameters E_o, E_d and E_g were found to be 6.84, 8.89, and 3.42 eV, respectively. The values of refractive index, $n(0)$, and the constant $\varepsilon_\infty = n(0)^2$ (for $h\nu \to 0$) extrapolated from the Wemple–DiDomenico model fit, and the high-frequency dielectric [23] are found equal $n(0) = 2.01$ and $\varepsilon_\infty = 4.04$.

The relation between the lattice dielectric constant ($\varepsilon_L = n^2$), wavelength (λ) and refractive index (n) is given by [24].

$$n^2 = \varepsilon_L - \left(\frac{e^2 N}{4\pi C^2 m*}\right)\lambda^2 \tag{7}$$

where ε_L is the lattice dielectric constant and N/m^* is ratio between the number of free carriers to the effective mass. The relation between n^2 and λ^2 is shown in Fig. 8 which verifies the linearity of

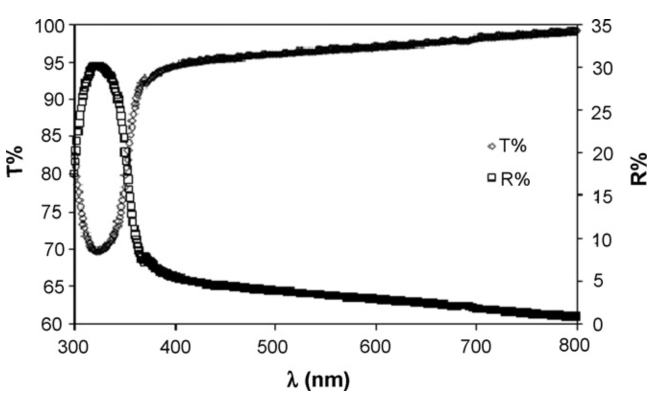

Fig. 5. The spectral distribution of transmittance (T%) and reflectance (R%) of NiO thin film.

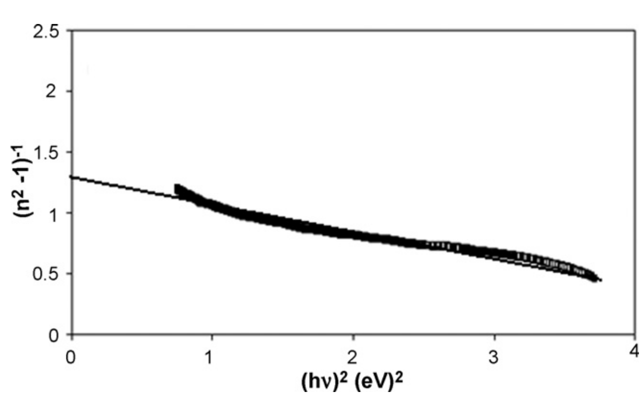

Fig. 7. The relation between $(n^2-1)^{-1}$ against $(h\nu)^2$ for NiO thin film.

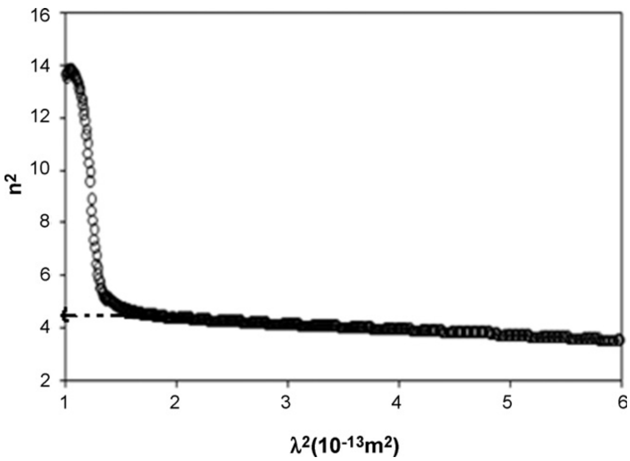

Fig. 8. The relation between n^2 and λ^2 for NiO thin film.

Eq. (7). The values of ε_L and (N/m^*) are determined from the extrapolation of these plots to $\lambda^2 = 0$ and from the slopes of the graphs and was found equal 4.3 and 2.3×10^{35} kg^{-1} m^{-3}, respectively. It is clear from the results that $(\varepsilon_\infty < \varepsilon_L)$, this is due to free charge carriers contribution in the polarization process that is occur inside the material when the light incident on it.

The third order of nonlinear polarizability parameter, $\chi^{(3)}$, so-called nonlinear optical susceptibility, is an important parameter, because it gives an indication about the strength of the chemical bonds between molecules of the prepared nanocrystalline thin film. The third-order nonlinear susceptibility of NiO film is calculated by using Eq. (8) [25], the spectrum is shown in Fig. 9.

$$\chi^{(3)} = A(\chi^{(1)})^4 = \frac{A}{(4\pi)^4(n^2-1)^4} = A\left(\frac{E_o E_d}{4\pi[E_o^2 - (h\nu)^2]}\right) \tag{8}$$

where A is a constant, $A = 1.7 \times 10^{-10}$ esu and $\chi^{(1)}$ is the linear optical susceptibility. Since the covalence and ionic chemical bonds strongly influence the magnitude of the nonlinearity. One can see that $\chi^{(3)}$ begins from 0.2×10^{-13} esu and get increase as the photon energy $h\nu$ increases up to 1.7 eV, after which $\chi^{(3)}$ has a limit value of 1.62×10^{-13} esu.

The obtained absolute values of transmittance and reflectance are used to determine the complex refractive index $(n^* = n - ik)$ and the complex dielectric constant $(\varepsilon^* = \varepsilon_1 - i\varepsilon_2)$ (where the real dielectric constant $\varepsilon_1 = (n^2 - k^2)$ and the imaginary dielectric constant $\varepsilon_2 = 2nk$). The real part generally relates to dispersion, while the imaginary part provides a measure to the dissipative rate of the wave in the medium [26]. Fig. 10 represents the variation of ε_1 and ε_2 with the photon energy for NiO thin film. As observed, the real and imaginary parts show maxima related to the absorption value. It is also possible to calculate the volume and surface energy loss functions (VELF and SELF) by using Eqs. (9) and (10) [27] and plotted in Fig. 11.

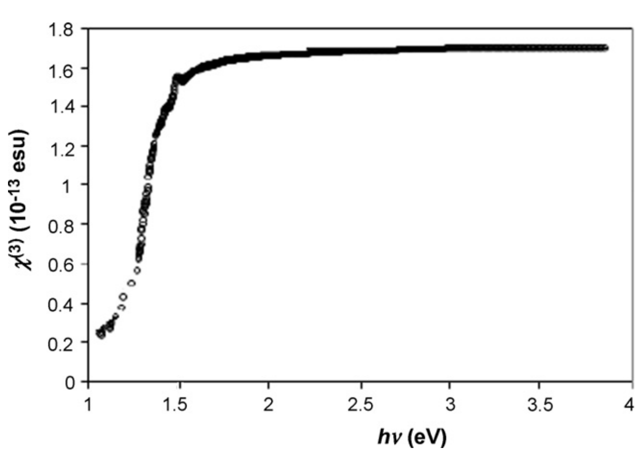

Fig. 9. The nonlinear optical susceptibility ($\chi^{(3)}$) as a function of photon energy ($h\nu$).

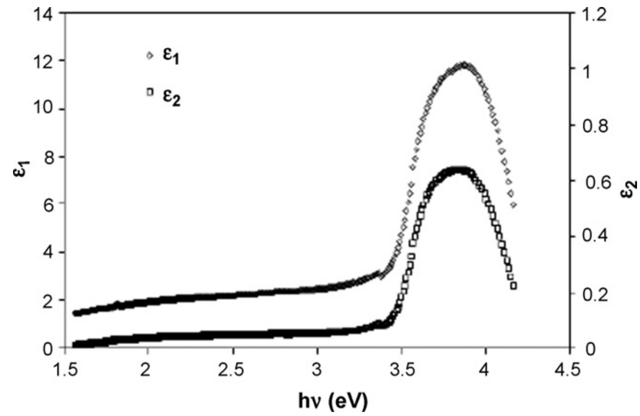

Fig. 10. The variation of ε_1 and ε_2 with the photon energy for NiO thin film.

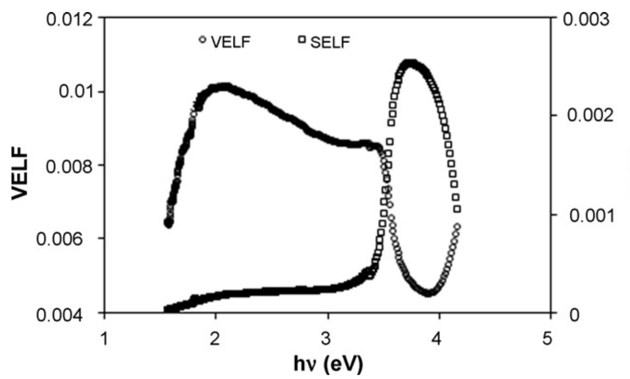

Fig. 11. The variation of VELF and SELF with the photon energy for NiO thin film.

$$\mathrm{VELF} = \frac{\varepsilon_2}{\varepsilon_1^2 + \varepsilon_2^2} \tag{9}$$

$$\mathrm{SELF} = \frac{\varepsilon_2}{[(\varepsilon_1 + 1)^2 + \varepsilon_2^2]} \tag{10}$$

From such figure, it is clear that the volume energy loss is greater than surface energy loss at all incident photon energies. It is also clear that the maximum of SELF and minimum of VELF corresponds to the absorption energy due to interband transition that occurs at 320 nm (3.9 eV).

4. Conclusion

NiO thin film has been deposited on a glass substrate by sol–gel process and spin-coating method. X-ray diffraction showed that it is a nanocrystalline structure. SEM revealed that the nanoparticles are extra-fine, with an average particle size of about 22 ± 3 nm. The optical band energy gap of the film is estimated at 3.44 eV. The dispersion of the refractive index in the film follows the single electronic oscillator mode. Using this model, the values obtained for the oscillator strength (E_d) and the oscillator energy (E_o) are 8.89 and 6.84 eV, respectively. The dielectric constant ε_∞ is evaluated to 4.04, the refractive index is equal at 2.01. The third-order nonlinear susceptibility $\chi^{(3)}$ is calculated using Frumer model, and is estimated to be 1.62×10^{-13} esu. The values of volume energy loss of NiO thin film was found greater than surface energy loss at all incident photon energies. It is also clear that the maximum of SELF and minimum of VELF corresponds to the absorption energy due to interband transition that occurs at 320 nm (3.9 eV).

References

[1] C.C. Chen, A.B. Herhold, C.S. Johnson, A.P. Alivisatos, Science 276 (1997) 398.
[2] Y. Wang, J. Zhu, X. Yang, L. Lu, X. Wang, Thermochim. Acta 437 (2005) 106.
[3] Y.R. Uhm, J.H. Park, W.W. Kim, C.H. Cho, C.K. Rhee, Mater. Sci. Eng. B 106 (2004) 224.
[4] S.H. Lin, F.R. Chen, J.J. Kai, Appl. Surf. Sci. 254 (2008) 3357.
[5] X. Wang, J. Song, L. Gao, J. Jin, H. Zheng, Z. Zhang, Nanotechnology 16 (2005) 37.
[6] H. Sato, T. Minami, S. Takata, T. Yamada, Thin Solid Films 236 (1993) 27.
[7] V. Srinivasan, J. Weidner, J. Electrochem. Soc. 144 (1997) L210.
[8] J. He, H. Lindström, A. Hagfeldt, S.E. Lindquist, J. Phys. Chem. B 103 (1999) 8940.
[9] R. Cinnsealach, G. Boschloo, S.N. Rao, D. Fitzmaurice, Sol. Energy Mater. Sol. Cells 57 (1999) 107.
[10] K. Yoshimura, T. Miki, S. Tanemura, Jpn. J. Appl. Phys. 34 (1995) 2440.
[11] C. Natarajan, H. Matsumoto, G. Nogami, J. Electrochem. Soc. 144 (1997) 121.
[12] C.S. Carney, C.J. Gump, A.W. Weimer, Mater. Sci. Eng. A 431 (2006) 1.
[13] A. Surca, B. Orel, B. Pihlar, P. Bukovec, J. Electroanal. Chem. 408 (1996) 83.
[14] D. Yang, R. Wang, M. He, J. Zhang, Z. Liu, J. Phys. Chem. B 109 (2005) 7654.
[15] W.E. Mahmoud, H. El-Mallah, J. Phys. D: Appl. Phys. 42 (2009) 035502.
[16] D.R. Sahu, Microchem. J. 38 (2007) 1252.
[17] L.E. Brus, J. Chem. Phys. 80 (1984) 4403.
[18] P. Singh, A.K. Chawla, D. Kaur, R. Chandra, Mater. Lett. 61 (2007) 2050.
[19] N.A. Subrahamanyam, A Textbook of Optics, 9th ed., Brj Laboratory, India, 1977.
[20] G. Hirankumar, S. Selvasekarapandian, N. Kuwata, J. Kawamura, T. Hattori, J. Power Sources 144 (1) (2005) 262.
[21] N. Tigau, V. Ciopina, G.I. Rusu, G. Prodan, E. Vasile, Romanian J. Phys. 50 (2005) 859.
[22] S.H. Wemple, M.D. DiDomenico Jr., Phys. Rev. B 3 (1970) 1338.
[23] H.S. Soliman, D.A. Abdel Hady, K.F. Abdel Rahman, S.B. Youssef, A.A. El-Shazly, Phys. A: Stat. Theo. Phys. 216 (1) (1995) 77.
[24] M.M. El-Nahass, Z. El-Gohary, H.S. Soliman, Opt. Laser Technol. 35 (2003) 523.
[25] T. Wagner, M. Krbal, T. Kohoutek, V. Peina, M. Vlek, M. Vlek, M. Frumar, J. Non-Cryst. Sol. 326 (2003) 233.
[26] G.A. Kumar, J. Thomas, N. George, B.A. Kumar, P. Radhakri, V.P.N. Shnan, C.P.G. Poori, N.V. Vallabhan, Unnikrishnan, Phys. Chem. Glass 41 (2000) 89.
[27] K.R. Rajesh, C.S. Menon, Mater. Lett. 53 (2002) 329.